Received: 31 January 2022 | Revised: 20 August 2022 | Accepted: 23 August 2022

DOI: 10.1002/rcm.9383

RESEARCH ARTICLE

Rapid Communications in Mass Spectrometry WILEY

Improved in situ analysis of lead isotopes in low-Pb melt inclusions using laser ablation–multi-collector–inductively coupled plasma–mass spectrometry

Hongxia Yu[1,2] | Yinhui Zhang[1] | Xijun Liu[1] | Lubing Hong[1,3,4] | Le Zhang[5] | Jifeng Xu[1,6] | Zhongyuan Ren[5] | Faliang Deng[1]

[1]Guangxi Key Laboratory of Hidden Metallic Ore Deposits Exploration, Guilin University of Technology, Guilin, China

[2]State Key Laboratory of Continental Dynamics, Northwest University, Xi'an, China

[3]Southern Marine Science and Engineering Guangdong Laboratory (Guangzhou), Guangzhou, China

[4]Collaborative Innovation Center for Exploration of Nonferrous Metal Deposits and Efficient Utilization of Resources by the Province and Ministry, Guilin University of Technology, Guilin, China

[5]State Key Laboratory of Isotope Geochemistry, Guangzhou Institute of Geochemistry, Chinese Academy of Sciences, Guangzhou, China

[6]School of Earth Sciences and Resources, and State Key Laboratory of Geological Processes and Mineral Resources, China University of Geosciences, Beijing, China

Correspondence
Y. Zhang and X. Liu, Guangxi Key Laboratory of Hidden Metallic Ore Deposits Exploration, Guilin University of Technology, Guilin 541006, China.
Email: zhangyinhui@glut.edu.cn and
Email: xijunliu@glut.edu.cn

Funding information
Bagui Scholar Innovation Project of Guangxi Province, Grant/Award Number: 2018XU Jifeng; Guangxi Key Laboratory of Hidden Metallic Ore Deposits Exploration, Grant/Award Numbers: GKY20-065-17-07, GKY20-065-17-08; Guangxi Natural Science Foundations of China, Grant/Award Number: GuikeAD22035160; Guilin University of Technology, Grant/Award Numbers: GUTQDJJ 2020015, GUTQDJJ 2019190; Key Special Project for Introduced Talents Team of Southern Marine Science and Engineering Guangdong Laboratory (Guangzhou), Grant/Award Number: GML2019ZD0202; NSFC, Grant/Award Numbers: 92055208, 42172053, 42002057; the Guangxi Science Innovation Base Construction Foundation, Grant/Award Number: GuikeZY21195031

Rationale: In situ Pb isotope analyses of tiny melt inclusions using laser ablation–multi-collector–inductively coupled plasma–mass spectrometry (LA–MC–ICP–MS) are crucial for exploring the origins of mafic lavas. However, quantitative use of this technique with low-Pb (<10 ppm) melt inclusions is difficult due to their low ^{204}Pb content and ^{204}Hg interference.

Methods: Pb isotopic ratios of various reference glasses and olivine-hosted melt inclusions were determined using LA–MC–ICP–MS. Multiple ion counters were used to simultaneously determine signal intensities of all Pb isotopes and ^{202}Hg. An Hg signal-removal smoothing device reduced its signal in the gas blank by >80%. Instrumental mass bias was corrected using the standard–sample bracketing method.

Results: With 24–90 μm diameter laser spots, 2–4 Hz repetition rates, and 2.5–4 J cm^{-2} energy fluence, the analytical precisions of ^{20x}Pb/^{204}Pb ratios ($x = 6, 7, 8$) for standards BHVO-2G, ML3B-G, NIST 614, NKT-1G, T1-G, GOR132-G, and StHs6/80-G were <1.0% (2RSD) when ^{208}Pb signals >100 000 cps. The Wangjiadashan melt inclusions have ^{206}Pb/^{204}Pb = 17.14–18.44, ^{207}Pb/^{204}Pb = 15.28–15.66, and ^{208}Pb/^{204}Pb = 37.12–38.68.

Conclusions: The described method improves the precision and accuracy of in situ Pb isotope analysis in low-Pb melt inclusions using LA–MC–ICP–MS. The Pb isotopic compositions of the Wangjiadashan melt inclusions indicate the coexistence of LoMu and EMII+young HIMU components in the mantle source of weakly alkaline basalts.

1 | INTRODUCTION

Melt inclusions are melt droplets, typically <100 μm in diameter, that are trapped in crystals during mineral growth.[1,2] They are physically isolated from most interaction with the external environment and record complex information on magma evolution, such as crystal fractionation, magma mixing, and crustal contamination; therefore, they have potential applications in exploring the petrogenesis of mantle-derived magmas.[3] Lead is concentrated mainly in the crust and is extremely depleted in the mantle[4,5] due to its highly incompatible and fluid-mobile behavior,[6,7] and it is useful in discerning whether the recycled crust is present in the mantle.[8] The three radiogenic Pb isotopic ratios ($^{20x}Pb/^{204}Pb$, where $x = 6, 7, 8$) are useful in characterizing mantle heterogeneity and determining the origin of recycled crust,[9–11] with the Pb isotopic compositions of melt inclusions being helpful in elucidating the origin of mafic magma.[12]

In situ analytical methods are widely applied in determining compositions of small targets such as melt inclusions,[3,13] with such Pb isotope analyses involving mainly secondary-ion mass spectrometry (SIMS) and laser ablation–multicollector–inductively coupled plasma–mass spectrometry (LA–MC–ICP–MS).[3] However, for low-Pb (<10 ppm) samples, both methods fail to obtain accurate $^{20x}Pb/^{204}Pb$ data, owing to the low ^{204}Pb abundance (~1.5 wt.%) in the Pb isotope system. The SIMS method usually ablates samples so little that the low ^{204}Pb signal intensities of low-Pb samples are easily influenced by surface contamination, and in the LA–MC–ICP–MS method, carrier gases may introduce traces of Hg, increasing the isobaric interference of ^{204}Hg on ^{204}Pb signal intensities.

As a result, current in situ high-precision Pb isotopic compositions of melt inclusions are generally reported as $^{20y}Pb/^{206}Pb$ ($y = 7, 8$)[13–15] but $^{20x}Pb/^{204}Pb$ ratios are rarely reported.[16,17] Although $^{20y}Pb/^{206}Pb$ ratios of melt inclusions are often used to infer mantle components (EMI, EMII, HIMU, and DMM) in sources of basalts,[13–15] they would fail to discriminate the LoMu (low-μ, where $\mu = ^{238}U/^{204}Pb$) from the EMI, because these two components share similarly high $^{20y}Pb/^{206}Pb$ ratios.[18] Nonetheless, the LoMu has much lower $^{208}Pb/^{204}Pb$ and $^{207}Pb/^{204}Pb$ at given $^{206}Pb/^{204}Pb$ than the EMI,[18] and therefore, can be easily discerned if the $^{20x}Pb/^{204}Pb$ ratios were obtained. Here, a highly efficient Hg-removal device with >80% Hg filtering in the gas blanks was employed, enabling the development of a protocol for in situ Pb isotope analyses, including the determination of the $^{20x}Pb/^{204}Pb$ ratios of small (<100 μm) and low-Pb samples using LA–MC–ICP–MS. The method was applied to determine the Pb isotopic compositions of olivine-hosted melt inclusions in the Wangjiadashan basalts from Shandong Province in eastern China.

2 | EXPERIMENTS

2.1 | Instrumentation

All analyses were carried out in a 193 nm COMPexPro 102 ArF excimer LA system (GeoLas HD, Gottingen, Germany) coupled to a Neptune Plus MC–ICP–MS (Thermo Fisher Scientific, Bremen, Germany) at the Guangxi Key Laboratory of Hidden Metallic Ore Deposits Exploration, Guilin University of Technology, Guilin, China. LA conditions included repetition rates of 2–4 Hz, energy fluences of 2.5–4 J cm^{-2}, and laser spot sizes of 24–90 μm (depending on Pb contents of samples). Helium was used as the carrier gas (650 ml min^{-1}). Each spot analysis included 23 s gas-blank collection and 30 s sample signal collection. To improve MC–ICP–MS sensitivity, a Jet sample cone and X skimmer cone were used. The ion beam intensities of ^{202}Hg, $^{204}(Pb + Hg)$, ^{206}Pb, ^{207}Pb, ^{208}Pb, ^{232}Th, and ^{238}U were determined simultaneously using seven ion counters (ICs). The instrument parameters are summarized in Table 1.

2.2 | Samples

2.2.1 | Glass standards

Nine international reference glasses with compositions ranging from ultramafic to granitic were used to evaluate the analytical accuracy and precision of the method. These reference glasses included three US Geological Survey (USGS) reference glasses (BHVO-2G, 1.73 ppm Pb; NKT-1G, 3.01 ppm Pb; BCR-2G, 11.0 ppm Pb), five MPI (Max Planck Institute, Germany)–DING reference glasses (KL2-G, 2.07 ppm Pb; ML3B-G, 1.38 ppm Pb; T1-G, 11.6 ppm Pb; GOR132-G, 19.5 ppm Pb; StHs6/80-G, 10.3 ppm Pb), and one US National Institute of Standards and Technology (NIST) reference glass (NIST 614, 2.32 ppm Pb; Table 2). The USGS and MPI–DING glasses comprise natural rock powders, and the NIST glass is a synthetic standard.[19,24] The reference glasses were mounted on epoxy discs, ground using coarse diamond powder of maximum particle size 0.5–5 μm, polished using a flannelette plate sprayed with 0.25 μm diamond solution, wiped with ethanol, and finally cleaned with distilled water in an ultrasonic bath prior to analysis.

2.2.2 | Sample description and olivine-hosted glassy melt inclusions

The Shandong Province is located in the central part of eastern China where the subducted Pacific Plate stagnates within the mantle transitional zone horizontally over >1000 km from the western Pacific subduction zone,[25] and crust–mantle interactions are widespread in the deep mantle.[26] Cenozoic basalts in this region can be classified into strongly and weakly alkaline basalts based on their petrological and geochemical compositions.[27–29] The strongly alkaline basalts were mainly formed at ages of <10 Ma with SiO_2 <43 wt.% and ($Na_2O + K_2O$) >6 wt.%; they have trace-element compositions similar to HIMU ocean-island basalt (OIB) but depleted Sr–Nd–Pb–Hf and extremely abnormal Mg-Zn isotopic compositions.[27–33] These unique compositions suggest sedimentary carbonate-modified young recycled oceanic crust in mantle source that was likely detached from the Pacific stagnant within the mantle transitional zone.[26,28–31] The weakly alkaline basalts were primarily formed at ages of 23–10 Ma with SiO_2 >43 wt.% and ($Na_2O + K_2O$) <6 wt.%; their trace-element and isotopic compositions resembled those of the EMI–OIB, indicating an EMI component in the mantle source.[26,28–30,33–35]

The Wangjiadashan basalts were collected at the northern part of the Tanlu fault in Shandong. These basalts are of porphyritic texture with large olivine phenocrysts (0.5–2 mm) in matrix of

TABLE 1 Operating parameters of the Neptune Plus ICP–MS and laser ablation systems

(a) Neptune Plus collector configuration for Pb-isotope analysis

Collector[a]	IC4	IC5	IC3	IC2	IC1	C	IC6	IC7
Mass	^{202}Hg	$^{204}(Pb + Hg)$	^{206}Pb	^{207}Pb	^{208}Pb	224.10	^{232}Th	^{238}U

(b) Typical instrument operating conditions

Neptune Plus MC-ICP-MS	
Instrument RF power	1220 W
Auxiliary gas (Ar)	0.94 L min^{-1}
Sample gas (Ar)	0.935 L min^{-1}
Cooling gas (Ar)	16 L min^{-1}
Measurement mode	Static
Interface cones	Jet sample cone and X skimmer cone
Acceleration voltage	10 kV
Detection system	Seven ion counters
Integration time	0.262 s
GeoLas HD laser ablation system	
Beam	UV193nm (ArF excimer)
Spot size	24/32/44/60/90 μm
Repetition rate	2–4 Hz
Energy density	2.5–4 J cm^{-2}
Ablation time	30s
Blank time	23 s
He gas to cell	650 mL min^{-1}
N_2 gas to cell	2–3 mL min^{-1}

[a]Collectors IC1 to IC7 are ion counters, and C is the center Faraday cup.

TABLE 2 Pb contents and isotopic ratios of the standard glasses used in this study

Standard glass	Pb (ppm)	$^{208}Pb/^{206}Pb$	2SD	$^{207}Pb/^{206}Pb$	2SD	$^{208}Pb/^{204}Pb$	2SD	$^{207}Pb/^{204}Pb$	2SD	$^{206}Pb/^{204}Pb$	2SD
NIST 614	2.32	2.1013		0.8710		37.47		15.53		17.83	
BHVO-2G	1.70	2.0499		0.8330		38.25		15.54		18.66	
BCR-2G	11.0	2.0639	0.0020	0.8327	0.0020	38.73	0.04	15.63	0.01	18.77	0.01
GOR132-G	19.5	2.0080	0.0050	0.8166	0.0026	38.72		15.72		19.25	
KL2-G	2.07	2.0227	0.0016	0.8212	0.0007	38.51	0.05	15.63	0.01	19.04	0.01
ML3B-G	1.38	2.0524	0.0020	0.8323	0.0020	38.42	0.15	15.58	0.10	18.72	0.04
StHs6/80-G	10.3	2.0379	0.0031	0.8263	0.0010	38.52	0.08	15.62	0.02	18.90	0.01
T1-G	11.6	2.0809	0.0002	0.8370	0.0007	38.98	0.01	15.68	0.02	18.73	0.01
NKT-1G	3.01	1.9992		0.7955		39.22		15.60		19.62	

Note: Sources of preferred Pb contents and Pb isotopic ratios: NIST 614[19]; BHVO-2G[20]; BCR-2G[20]; GOR132-G, KL2-G, ML3B-G, StHs6/80-G, and T1-G[21]; and NKT-1G.[22,23]

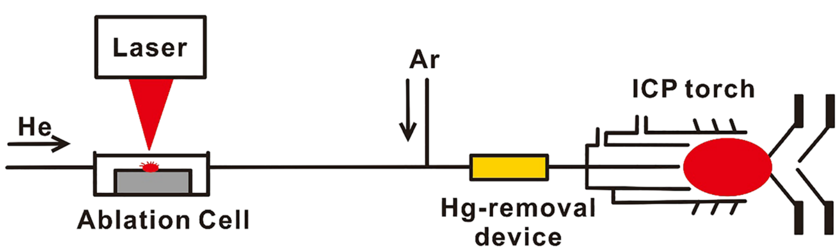

FIGURE 1 Schematic diagram of laser ablation–multi-collector–inductively coupled plasma–mass spectrometry [Color figure can be viewed at wileyonlinelibrary.com]

pyroxene, plagioclase, olivine, and magnetite. They are weakly alkaline basalts with 46.8–47.7 wt.% SiO_2, 3.4–4.6 wt.% ($Na_2O + K_2O$), 7.7–10.5 wt.% MgO, and EMI-OIB's trace element compositions. Different from the whole-rock compositions, their melt inclusions exhibit large ^{20y}Pb/^{206}Pb isotopic variations, ranging from the Pb isotopic compositions of the strong to weakly alkaline basalts. Detailed information including sample location, petrology, and geochemistry of the Wangjiadashan basalts has been reported by Zhang et al.[36]

Olivines were collected from the Cenozoic Wangjiadashan basalts of Shandong, eastern China, and were heated for ~10 min in a 1-atm gas-mixing furnace at 1250°C with an oxygen fugacity of the quartz–fayalite–magnetite buffer, following the procedure of Ren et al,[37] then quickly quenched to ~25°C to obtain glassy melt inclusions. The resulting olivine grains were mounted in epoxy resin and polished until the inclusions were exposed at the surface. All procedures were completed at the State Key Laboratory of Isotope Geochemistry, Guangzhou Institute of Geochemistry, Chinese Academy of Sciences, Guangzhou, China.

2.3 | Mercury-removal device

Accurate determination of the intensity of ^{204}Pb signals is critical but difficult for high-precision Pb isotope analyses of low-Pb samples because the ^{204}Pb content is much lower than those of ^{206}Pb, ^{207}Pb, and ^{208}Pb, and there may be signal interference by ^{204}Hg from the carrier gas (He), sample gas (Ar), or auxiliary gases (N_2, Ar) during analysis.[13,16] Here, a Hg-removal signal-smoothing device developed by Hu et al[38] was used to reduce the Hg influence on ^{204}Pb signal intensity, allowing the accurate determination of ^{204}Pb signal intensity. This device comprises a steel cylinder filled with Au-coated corrugated plates[38] and was placed in the front of ICP torch (Figure 1) to reduce Hg signals in the He and sample gas. Using this Hg-removal signal-smoothing device, ^{202}Hg background was reduced from ~20 000 to 2000–3700 cps, corresponding to a reduction in ^{204}Hg background from 2300–4600 to 450–850 cps, assuming ^{204}Hg/^{202}Hg = 0.2301.[39] The ^{204}Pb intensity was obtained from the ^{204}(Pb + Hg) intensity by subtracting ^{204}Hg intensity.

2.4 | Mass-bias correction

Among the Pb isotopes, ^{206}Pb, ^{207}Pb, and ^{208}Pb are radiogenic; only ^{204}Pb is unradiogenic. For Pb isotope analysis, it is impossible to make a mass-bias correction between two unradiogenic isotopes, such as Sr, Nd, and Hf. For mass-bias correction, we used reference glasses KL2-G (2.07 ppm Pb) and BCR-2G (11 ppm Pb) for external correction of low-Pb (<5 ppm) and high-Pb (>10 ppm) samples, respectively. Analyses were undertaken for every unknown sample preceded and followed by analysis of one reference glass, with the mass-bias correction calculated as follows:

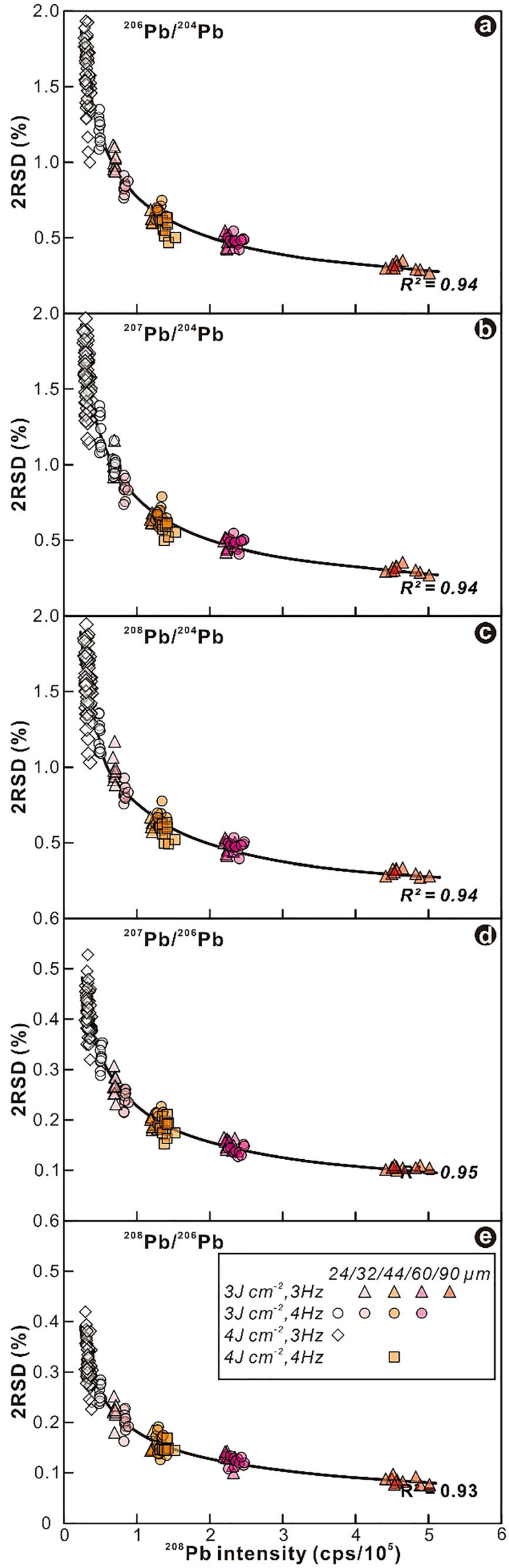

FIGURE 2 Plots of 2RSD values of Pb isotopic ratios vs. ^{208}Pb intensity for BHVO-2G under different laser ablation conditions [Color figure can be viewed at wileyonlinelibrary.com]

$$S_C = \frac{S_m}{(R_{m1} + R_{m1})/2/R} \quad (1)$$

where S_C and S_m are corrected and measured values of Pb isotopic ratios for the unknown sample, respectively; R_{m1} and R_{m2} are measured values for the reference glasses preceding and following the unknown sample, respectively; and R is the preferred reference value of the reference glass.

3 | RESULTS AND DISCUSSION

3.1 | Precision and accuracy for glass standards

Precision and accuracy are crucial to the evaluation of data quality, and to assess them we first analyzed the low-Pb USGS glass BHVO-2G (1.73 ppm Pb) with laser spot sizes of <100 μm, low energy fluences (3–4 J cm^{-2}), and low repetition rates (3–4 Hz). Results

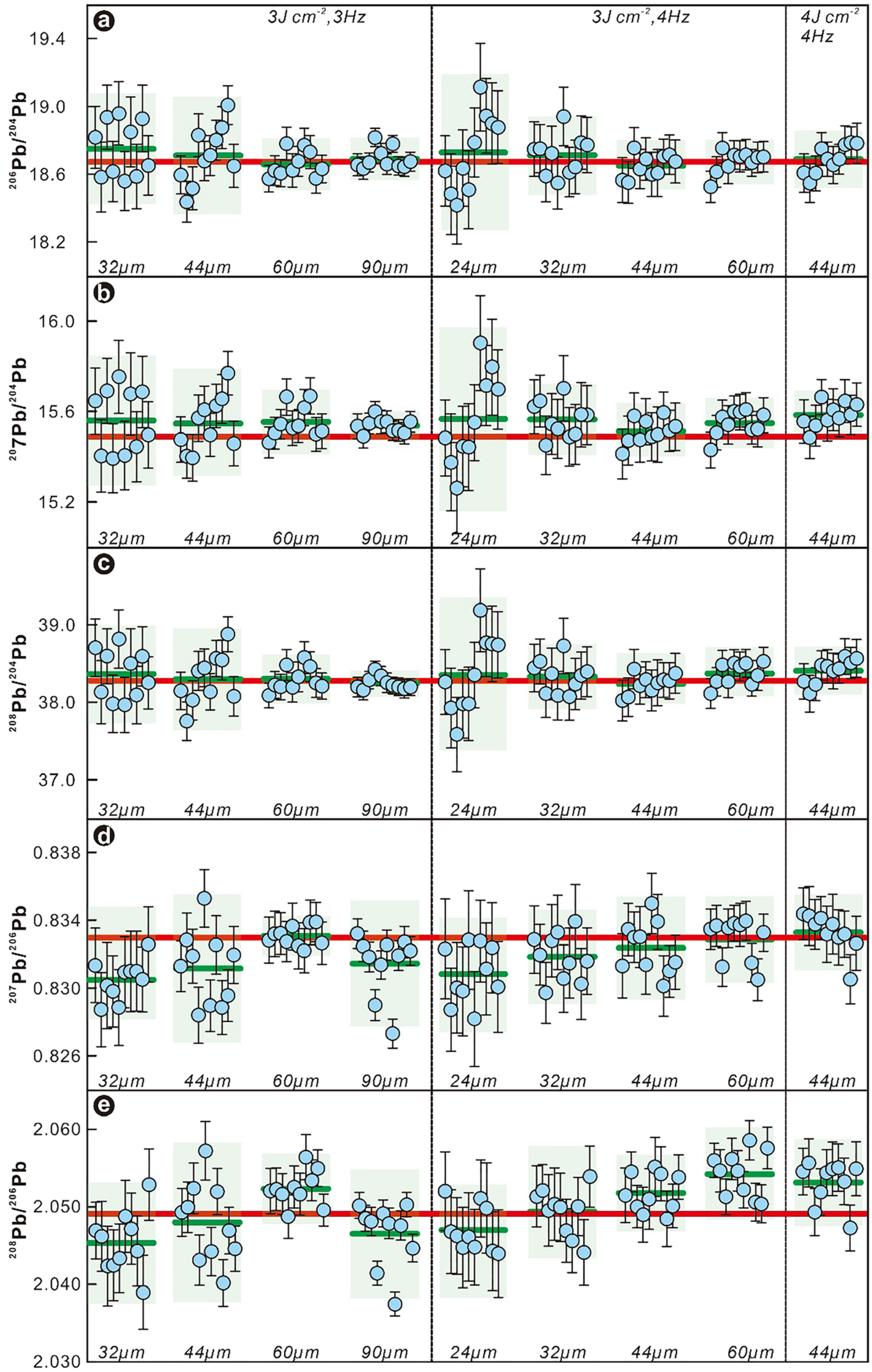

FIGURE 3 Precision and accuracy of $^{20x}Pb/^{204}Pb$ ($x = 6, 7, 8$) and $^{20y}Pb/^{206}Pb$ ($y = 7, 8$) ratios for BHVO-2G under different LA conditions. Red and green lines represent preferred and average values, respectively. Error bars are 2SD [Color figure can be viewed at wileyonlinelibrary.com]

(Figure 2) show that with increasing spot size, energy fluence, and repetition rate, the ^{208}Pb signal intensity increases from 30 000 to 500 000 cps, with two relative standard deviation (2RSD) values of $^{20x}Pb/^{204}Pb$ and $^{20y}Pb/^{206}Pb$ ratios decreasing from 2.0% to 0.3% and from 0.6% to <0.1%, respectively. The 2RSD values of $^{20x}Pb/^{204}Pb$ and $^{20y}Pb/^{206}Pb$ ratios and the ^{208}Pb signal intensity

TABLE 3 Pb isotopic ratios of BHVO-2G determined using different laser ablation parameters in this study

Spot size (μm)		$^{208}Pb/^{206}Pb$	$^{207}Pb/^{206}Pb$	$^{208}Pb/^{204}Pb$	$^{207}Pb/^{204}Pb$	$^{206}Pb/^{204}Pb$
Repetition rate = 3 Hz; energy density = 3 J cm^{-2}; ablation time = 30 s						
32	Average (n = 10)	2.0454	0.8305	38.37	15.56	18.75
	2SD	0.0078	0.0023	0.63	0.29	0.33
	2RSD	0.38%	0.28%	1.64%	1.85%	1.75%
	Accuracy	−0.22%	−0.30%	0.31%	0.12%	0.49%
44	Average (n = 10)	2.0480	0.8312	38.30	15.55	18.71
	2SD	0.0103	0.0044	0.66	0.24	0.35
	2RSD	0.50%	0.53%	1.71%	1.55%	1.85%
	Accuracy	−0.09%	−0.22%	0.14%	0.03%	0.29%
60	Average (n = 10)	2.0523	0.8331	38.31	15.56	18.66
	2SD	0.0045	0.0012	0.31	0.14	0.15
	2RSD	0.22%	0.14%	0.82%	0.92%	0.82%
	Accuracy	0.12%	0.01%	0.14%	0.08%	0.01%
90	Average (n = 10)	2.0465	0.8315	38.25	15.54	18.69
	2SD	0.0083	0.0037	0.17	0.06	0.12
	2RSD	0.41%	0.45%	0.44%	0.41%	0.67%
	Accuracy	−0.16%	−0.18%	0.00%	−0.03%	0.18%
Repetition rate = 3 Hz; energy density = 4 J cm^{-2}; ablation time = 30 s						
24	Average (n = 60)	2.049	0.832	38.40	15.59	18.75
	2SD	0.008	0.004	1.44	0.57	0.69
	2RSD	0.41%	0.54%	3.76%	3.63%	3.66%
	Accuracy	−0.04%	−0.15%	0.39%	0.29%	0.46%
Repetition rate = 4 Hz; energy density = 3 J cm^{-2}; ablation time = 30 s						
24	Average (n = 10)	2.0470	0.8309	38.36	15.57	18.73
	2SD	0.0059	0.0034	1.00	0.41	0.46
	2RSD	0.29%	0.41%	2.60%	2.61%	2.45%
	Accuracy	−0.14%	−0.26%	0.28%	0.17%	0.39%
32	Average (n = 10)	2.0494	0.8319	38.34	15.57	18.71
	2SD	0.0060	0.0028	0.42	0.16	0.23
	2RSD	0.29%	0.33%	1.10%	1.00%	1.24%
	Accuracy	−0.02%	−0.14%	0.22%	0.15%	0.29%
44	Average (n = 10)	2.0518	0.8324	38.24	15.51	18.65
	2SD	0.0049	0.0030	0.26	0.11	0.14
	2RSD	0.24%	0.37%	0.67%	0.71%	0.74%
	Accuracy	0.09%	−0.07%	−0.02%	−0.18%	−0.04%
60	Average (n = 10)	2.0542	0.8329	38.38	15.55	18.68
	2SD	0.0059	0.0025	0.29	0.11	0.13
	2RSD	0.29%	0.31%	0.76%	0.71%	0.70%
	Accuracy	0.21%	−0.01%	0.33%	0.05%	0.09%
Repetition rate = 4 Hz; energy density = 4 J cm^{-2}; ablation time = 30 s						
44	Average (n = 10)	2.0531	0.8333	38.41	15.59	18.69
	2SD	0.0056	0.0023	0.31	0.11	0.17
	2RSD	0.27%	0.27%	0.81%	0.69%	0.90%
	Accuracy	0.16%	0.04%	0.42%	0.28%	0.17%

display clear exponential curve fits (Figure 2), consistent with previous observations.[13,16,40,41] Individual $^{20x}Pb/^{204}Pb$ and $^{20y}Pb/^{206}Pb$ ratios of BHVO-2G are more variable, with a smaller spot size, lower energy fluence, and lower repetition rate (Figure 3). The 2RSD of average $^{20x}Pb/^{204}Pb$ and $^{20y}Pb/^{206}Pb$ ratios are better than 3.8% and 0.6%, respectively, and accuracies are better than 0.5% and 0.3%, respectively. The accuracies of average $^{20x}Pb/^{204}Pb$ and $^{20y}Pb/^{206}Pb$ ratios are apparently insensitive to LA effects (Table 3).

Precision and accuracy were further evaluated by analysis of a further six glass standards. Three low-Pb (<5 ppm) glass standards (ML3B-G, 1.38 ppm; NIST 614, 2.32 ppm; NKT-1G, 3.01 ppm) were analyzed, with LA conditions of 44 μm spot size, 4 J cm^{-2} fluence, and 4 Hz repetition rate. A further three high-Pb (>10 ppm) glass standards (T1-G, 11.6 ppm; GOR132-G, 19.5 ppm; StHs6/80-G, 10.3 ppm) were analyzed with 32 μm spot size, 2–3 J cm^{-2} fluences, and 2.5–3 Hz repetition rates. Results indicate that these six glass standards have ^{208}Pb signal intensities of 100 000–450 000 cps, with 2RSD values for $^{20x}Pb/^{204}Pb$ and $^{20y}Pb/^{206}Pb$ ratios of 0.6%–0.3% and 0.3%–<0.1%, respectively (Figure FIGURE S1 [supporting information]). Their 2RSD values and

TABLE 4 Pb isotopic ratios of NIST614, NKT-1G, ML3B-G, KL2-G, StHs6/80G, and T1-G

Spot size (μm)	Repetition rate (Hz)	Energy density (J cm^{-2})	Ablation time (s)		$^{208}Pb/^{206}Pb$	$^{207}Pb/^{206}Pb$	$^{208}Pb/^{204}Pb$	$^{207}Pb/^{204}Pb$	$^{206}Pb/^{204}Pb$
NIST 614 (2.31 ppm Pb)									
44	4	4	30	Average (n = 10)	2.1096	0.8731	37.619	15.569	17.844
				2SD	0.0047	0.0015	0.292	0.106	0.129
				2RSD	0.22%	0.18%	0.78%	0.68%	0.72%
				Accuracy	0.39%	0.24%	0.39%	0.23%	0.06%
NKT-1G (3.01 ppm Pb)									
44	4	4	30	Average (n = 10)	2.0035	0.7966	39.306	15.632	19.626
				2SD	0.0048	0.0021	0.231	0.085	0.105
				2RSD	0.24%	0.26%	0.59%	0.55%	0.53%
				Accuracy	0.21%	0.13%	0.23%	0.18%	0.06%
ML3B-G (1.38 ppm Pb)									
44	4	4	30	Average (n = 10)	2.0522	0.8324	38.524	15.615	18.768
				2SD	0.0054	0.0027	0.296	0.114	0.113
				2RSD	0.26%	0.33%	0.77%	0.73%	0.60%
				Accuracy	−0.01%	0.02%	0.27%	0.22%	0.26%
KL-2G (2.07 ppm Pb)									
44	4	4	30	Average (n = 39)	2.0196	0.8203	38.443	15.613	19.037
				2SD	0.0094	0.0030	0.281	0.098	0.134
				2RSD	0.46%	0.37%	0.73%	0.63%	0.70%
				Accuracy	−0.15%	−0.11%	−0.17%	−0.13%	−0.01%
StHs6/80-G (10.3 ppm Pb)									
32	3	3	30	Average (n = 10)	2.0385	0.8264	38.624	15.650	18.940
				2SD	0.0021	0.0011	0.204	0.103	0.122
				2RSD	0.10%	0.13%	0.53%	0.66%	0.64%
				Accuracy	0.03%	0.02%	0.27%	0.21%	0.20%
T1-G (11.6 ppm Pb)									
32	3	3	30	Average (n = 10)	2.0813	0.837	39.004	15.694	18.741
				2SD	0.0033	0.002	0.152	0.070	0.091
				2RSD	0.16%	0.19%	0.39%	0.45%	0.49%
				Accuracy	0.02%	−0.01%	0.07%	0.10%	0.05%
GOR132-G (19.5 ppm Pb)									
32	2.5	2	30	Average (n = 10)	2.0074	0.8167	38.738	15.762	19.303
				2SD	0.0032	0.0011	0.288	0.116	0.131
				2RSD	0.16%	0.14%	0.74%	0.74%	0.68%
				Accuracy	−0.03%	0.01%	0.05%	0.27%	0.28%

Notes: Isotopic ratios of NIST 614, BHVO-2G, NKT-1G, and ML3B-G were corrected by preferred isotopic ratios of KL-2G; those of KL-2G were corrected by preferred isotopic ratios of NKT-1G; and those of StHs6/80-G, T1-G, and GOR132-G were corrected by preferred Pb isotopic ratios of BCR-2G.

^{208}Pb signal intensities have exponential curve fits, as defined by the results for BHVO-2G. Considering the large compositional range of the glass standards, from ultramafic (GOR132-G) to dacitic (StHs6/80-G), and NIST 614, these results support there being no composition-related matrix effects at these levels of precision, with signal intensity playing the predominant role in analytical precision during Pb isotope analyses. The exponential curve fits (Figure 2 and Figure FIGURE S1 [supporting information]) indicate uncertainties in ^{20x}Pb/^{204}Pb and ^{20y}Pb/^{206}Pb ratios of better than 1.0% and 0.6%, respectively, when the ^{208}Pb intensity is >100 000 cps. The ML3B-G, NKT-1G, StHs6/80-G, T1-G, and GOR132-G standards have ^{20x}Pb/^{204}Pb and ^{20y}Pb/^{206}Pb ratios 2RSD of <0.8% and <0.5, respectively, and accuracies of <0.5% and <0.4%, respectively (Table 4; Figures S2 and S3 [supporting information]). The NIST 614 standard has slightly less-accurate Pb isotopic ratios (<0.8%; Table 4; Figures S2 and S3 [supporting information]). The Pb isotopic ratios for the analyzed geological reference glasses and their recommended values are positively correlated with $r^2 = 1.0$ (Figure 4).

3.2 | Comparison with other studies

Published data for in situ Pb isotope analyses of the glass standards (BHVO-2G, NKT-1G, ML3B-G, KL2-G, and T1-G) under similar LA conditions were compiled (Table 5). Faraday cups and ICs were applied by Paul et al[16] and Zhang et al[41] in determining ^{20x}Pb and ^{204}Pb intensities, respectively, whereas other studies[13,42] and the present study used ICs to determine ^{20x}Pb and ^{204}Pb intensities. To obtain high ^{208}Pb intensity, Paul et al,[16] Souders and Sylvester,[42] and Zhang et al[41] used either large laser spot sizes (90–93 μm) or high laser repetition rates (8–10 Hz), whereas Zhang et al[13] applied a 23 μm laser spot size, 3 Hz repetition rate, and 80 mJ energy with a 50% energy attenuator (4 J cm^{-2} fluence), similar to our study (24–44 μm laser spot size, 2.5–4 Hz repetition rate, and 2–4 J cm^{-2} fluence). LA conditions used by Zhang et al[13] are more suitable for determination of Pb isotopic ratios in tiny melt inclusions. However, the low ^{204}Pb signal intensity and relatively high ^{204}Hg isobaric interference led to low precision.[13] External precisions of Pb isotopic ratios between this and other studies are compared in Figure 5. All measurements have high external precisions for ^{20y}Pb/^{206}Pb ratios (2RSD < 1%). For ^{20x}Pb/^{204}Pb ratios, determined using 24 μm spot size and 3–4 Hz repetition rates, the external precisions of this study for BHVO-2G (2RSD = 2.6%–3.8%) are much improved over those of Zhang et al[13] (2RSD = 5.2%–5.5%) because of the low Hg background. For high-Pb (>10 ppm) samples such as T1-G (11.6 ppm), the ^{20x}Pb/^{204}Pb external precisions here (2RSD = ~0.5%) are comparable to those of analyses (2RSD = ~0.8%) involving larger spot sizes or higher repetition rates. For low-Pb (<5 ppm) samples such as KL2-G (2.07 ppm) and ML3B-G (1.38 ppm), the ^{20x}Pb/^{204}Pb external precisions (2RSD = ~0.7%) are significantly improved over those obtained with larger spot sizes or higher repetition rates (2RSD = 1.5%–2.5%).

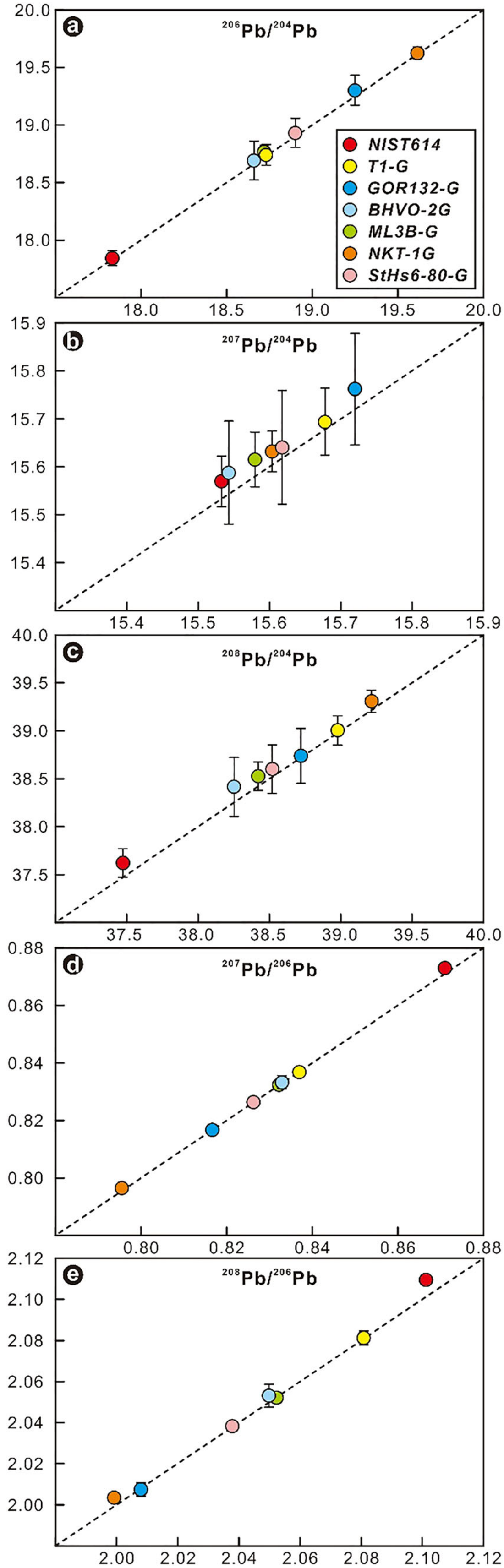

FIGURE 4 Comparison of measured and preferred Pb isotopic compositions of glass standards. Error bars are 2SD [Color figure can be viewed at wileyonlinelibrary.com]

TABLE 5 Comparison among studies of precision and accuracy of Pb isotopic compositions determined using LA–MC–ICP–MS

Detector	Spot size (μm)	Repetition rate (Hz)	Energy density (J cm^{-2})	Ablation time (s)		$^{208}Pb/^{206}Pb$ (%)	$^{207}Pb/^{206}Pb$ (%)	$^{208}Pb/^{204}Pb$ (%)	$^{207}Pb/^{204}Pb$ (%)	$^{206}Pb/^{204}Pb$ (%)	References
BHVO-2G (1.73 ppm Pb)											
IC	23	3	4	30	2RSD (n = 20)	0.60	0.50	5.50	5.30	5.20	1
					Accuracy	0.15	0.13	0.89	0.81	0.79	
IC	**24**	**3**	**4**	**30**	**2RSD (n = 60)**	**0.41**	**0.54**	**3.76**	**3.63**	**3.66**	**2**
					Accuracy	**−0.04**	**−0.15**	**0.39**	**0.29**	**0.46**	
IC	**24**	**4**	**3**	**30**	**2RSD (n = 10)**	**0.29**	**0.41**	**2.60**	**2.61**	**2.45**	**2**
					Accuracy	**−0.14**	**−0.26**	**0.28**	**0.17**	**0.39**	
IC	**32**	**3**	**3**	**30**	**2RSD (n = 10)**	**0.38**	**0.28**	**1.64**	**1.85**	**1.75**	**2**
					Accuracy	**−0.22**	**−0.30**	**0.31**	**0.12**	**0.49**	
IC	**44**	**4**	**4**	**30**	**2RSD (n = 10)**	**0.27**	**0.27**	**0.81**	**0.69**	**0.90**	**2**
					Accuracy	**0.08**	**0.04**	**0.42**	**0.28**	**0.17**	
NKT-1G (3.01 ppm Pb)											
IC	23	3	4	30	2RSD (n = 16)	0.39	0.35	3.04	3.13	3.13	1
					Accuracy	−0.17	0.02	−0.77	−0.60	−0.70	
IC	**44**	**4**	**4**	**30**	**2RSD (n = 10)**	**0.24**	**0.26**	**0.59**	**0.55**	**0.53**	**2**
					Accuracy	**0.21**	**0.13**	**0.23**	**0.18**	**0.06**	
ML3B-G (1.38 ppm Pb)											
IC	69	10	5	50	2RSD (n = 21)	0.53	0.34	2.71	2.73	2.73	3
					Accuracy	−0.21	0.89	−1.26	−1.36	−1.06	
IC	**44**	**4**	**4**	**30**	**2RSD (n = 10)**	**0.26**	**0.33**	**0.77**	**0.73**	**0.60**	**2**
					Accuracy	**−0.01**	**0.02**	**0.27**	**0.22**	**0.26**	
KL-2G (2.07 ppm Pb)											
Faraday-IC	93	6	5	60	2RSD (n = 20)	0.70	1.06	1.47	1.76	1.43	4
					Accuracy	0.01	−0.27	0.02	−0.09	0.03	
IC	69	10	5	50	2RSD (n = 21)	0.40	0.34	2.59	2.51	2.82	3
					Accuracy	0.23	0.02	0.19	−0.01	0.08	
IC	**44**	**4**	**4**	**30**	**2RSD (n = 39)**	**0.46**	**0.37**	**0.73**	**0.63**	**0.70**	**2**
					Accuracy	**−0.15**	**−0.11**	**−0.17**	**−0.13**	**−0.01**	

(Continues)

TABLE 5 (Continued)

Detector	Spot size (μm)	Repetition rate (Hz)	Energy density (J cm^{-2})	Ablation time (s)		$^{208}Pb/^{206}Pb$ (%)	$^{207}Pb/^{206}Pb$ (%)	$^{208}Pb/^{204}Pb$ (%)	$^{207}Pb/^{204}Pb$ (%)	$^{206}Pb/^{204}Pb$ (%)	References
T1-G (11.6 ppm Pb)											
IC	40	10	5	50	2RSD (n = 11)	0.36	0.22	0.83	0.78	0.70	3
					Accuracy	0.03	−0.04	0.02	−0.04	0.03	
IC	**32**	**3**	**3**	**30**	**2RSD (n = 10)**	**0.16**	**0.19**	**0.39**	**0.45**	**0.49**	**2**
					Accuracy	**0.02**	**−0.01**	**0.07**	**0.10**	**0.05**	

Notes: KL-2G was corrected by NKT-1G; precision and accuracy of Pb isotopic compositions measured in this study are shown in bold for comparison with those in other studies. References: 1[13]; 2, this study; 3[31]; 4.[16]

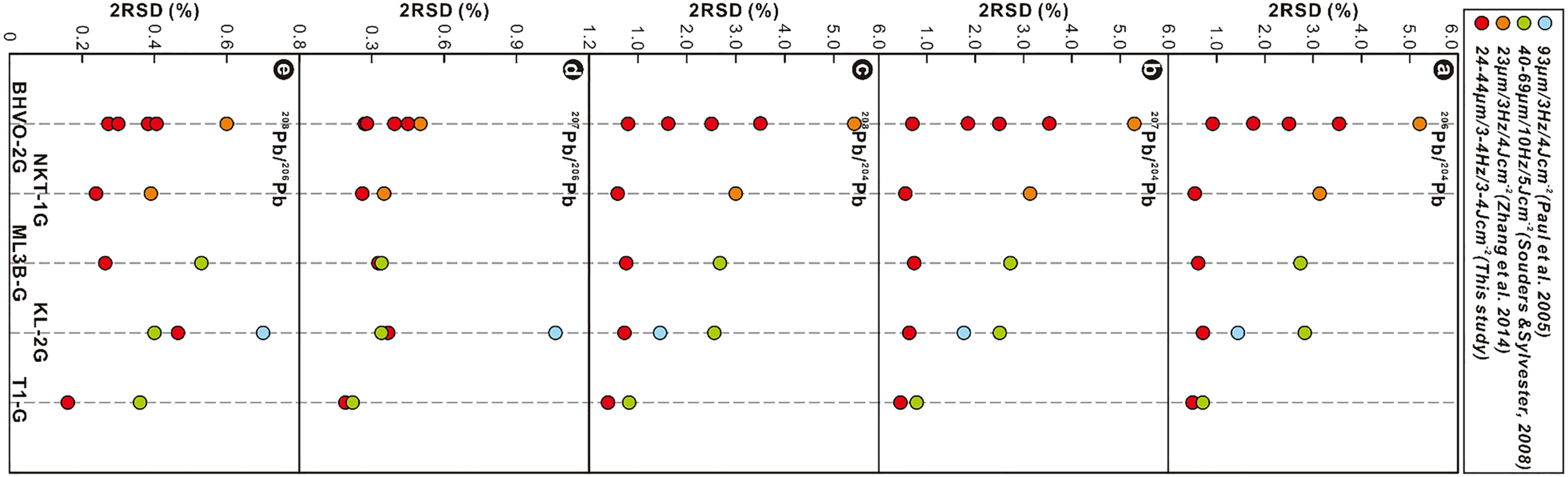

FIGURE 5 Comparison of the external precisions (2RSD) of Pb isotopic ratios from laser ablation–multi-collector–inductively coupled plasma–mass spectrometry analyses in this study with other studies [Color figure can be viewed at wileyonlinelibrary.com]

TABLE 6 Pb isotopic ratios of the Wangjiadashan melt inclusions determined in this study

Lava no.	Melt inclusion no.	$^{208}Pb/^{206}Pb$	2SE	$^{207}Pb/^{206}Pb$	2SE	$^{206}Pb/^{204}Pb$	2SE	$^{207}Pb/^{204}Pb$	2SE	$^{208}Pb/^{204}Pb$	2SE
DSW09-8	DSW09-8-15	2.100	0.004	0.851	0.002	18.40	0.12	15.66	0.11	38.68	0.26
	DSW09-8-19	2.099	0.004	0.852	0.002	18.32	0.10	15.60	0.09	38.38	0.22
	DSW09-8-20	2.101	0.004	0.849	0.002	18.21	0.12	15.49	0.11	38.25	0.25
	DSW09-8-24	2.105	0.003	0.856	0.002	18.29	0.12	15.65	0.10	38.43	0.24
	DSW09-8-50B	2.095	0.003	0.850	0.002	18.34	0.11	15.60	0.09	38.37	0.23
	DSW09-8-58	2.099	0.005	0.849	0.003	18.32	0.17	15.56	0.14	38.48	0.33
	DSW09-8-39	2.166	0.003	0.891	0.002	17.22	0.10	15.35	0.09	37.32	0.22
	DSW09-8-41	2.156	0.003	0.885	0.001	17.38	0.07	15.40	0.06	37.44	0.15
	DSW09-8-47	2.152	0.003	0.885	0.001	17.35	0.10	15.37	0.09	37.27	0.20
	DSW09-8-50	2.166	0.003	0.890	0.002	17.14	0.09	15.28	0.09	37.12	0.19
	DSW09-8-53	2.169	0.002	0.889	0.001	17.32	0.08	15.37	0.07	37.50	0.18
	DSW09-8-63	2.164	0.003	0.891	0.001	17.38	0.09	15.43	0.07	37.62	0.18
	DSW09-8-64	2.163	0.003	0.891	0.001	17.31	0.09	15.40	0.08	37.40	0.18
	DSW09-8-65	2.161	0.003	0.888	0.002	17.30	0.11	15.33	0.09	37.33	0.22
	DSW09-8-70	2.167	0.003	0.891	0.001	17.23	0.09	15.34	0.08	37.28	0.20
	DSW09-8-72	2.160	0.004	0.887	0.002	17.27	0.08	15.30	0.08	37.28	0.17
DSW09-12	DSW09-12-1	2.104	0.005	0.854	0.002	18.28	0.12	15.62	0.10	38.46	0.24
	DSW09-12-6	2.096	0.004	0.853	0.002	18.24	0.11	15.59	0.10	38.41	0.23
	DSW09-12-15	2.097	0.004	0.851	0.002	18.26	0.12	15.55	0.11	38.28	0.25
	DSW09-12-16	2.099	0.005	0.852	0.002	18.32	0.14	15.59	0.13	38.40	0.30
	DSW09-12-19	2.101	0.004	0.854	0.002	18.27	0.12	15.54	0.11	38.30	0.28
	DSW09-12-25	2.097	0.005	0.849	0.002	18.44	0.17	15.64	0.14	38.67	0.36
	DSW09-12-26	2.098	0.004	0.852	0.002	18.37	0.14	15.62	0.11	38.55	0.30
	DSW09-12-14	2.162	0.003	0.888	0.001	17.41	0.09	15.47	0.08	37.66	0.20
	DSW09-12-17	2.154	0.002	0.885	0.001	17.41	0.07	15.42	0.07	37.54	0.16
	DSW09-12-23	2.146	0.004	0.884	0.002	17.58	0.12	15.48	0.11	37.69	0.26
	DSW09-12-5	2.142	0.005	0.878	0.003	17.83	0.15	15.64	0.14	38.25	0.34
	DSW09-12-9	2.127	0.003	0.868	0.002	17.87	0.12	15.51	0.11	38.08	0.23
	DSW09-12-12	2.127	0.004	0.868	0.002	17.85	0.11	15.49	0.10	37.97	0.23

3.3 | Analysis of olivine-hosted melt inclusions in Wangjiadashan basalts

Pb isotopic ratios of 29 olivine-hosted melt inclusions from Cenozoic Wangjiadashan basalts in Shandong Province were determined using LA conditions of 44 μm spot size, 4 J cm^{-2} fluence, 4 Hz repetition rate, and 30 s ablation time. These melt inclusions have 70 000–270 000 cps ${}^{208}Pb$ intensities, lower than that of the NKT-1G standard (3.01 ppm Pb; ~340 000 cps ${}^{208}Pb$ intensity), indicating a Pb content of <3 ppm in the melt inclusions. The Pb isotopic ratios of the Wangjidashan melt inclusions are shown in Table 6 and Figure 6. The melt inclusions in sample DSW09-8 have ${}^{208}Pb/{}^{206}Pb$, ${}^{207}Pb/{}^{206}Pb$, ${}^{206}Pb/{}^{204}Pb$, ${}^{207}Pb/{}^{204}Pb$, and ${}^{208}Pb/{}^{204}Pb$ ratios of 2.095–2.169, 0.849–0.891, 17.14–18.44, 15.28–15.66, and 37.12–38.68, respectively: the melt inclusions with low ${}^{20x}Pb/{}^{206}Pb$ and high ${}^{20y}Pb/{}^{206}Pb$ similar to the LoMu component, whereas the ones with high ${}^{20x}Pb/{}^{206}Pb$ and low ${}^{20y}Pb/{}^{206}Pb$ close to the field of young HIMU component and EMII defined by Mid-Oceanic Ridge basalts (MORBs)[8] and pelagic sediments,[45] respectively. Such a large Pb isotopic range is also observed in the melt inclusions of sample DSW09-12.

Whole-rock compositions of the Cenozoic Shandong basalts have revealed highly geochemical heterogeneity in mantle source: sedimentary carbonate-modified young recycled oceanic crust indicated by the strongly alkaline basalts with HIMU-OIBs' trace-element compositions but depleted Sr–Nd–Pb–Hf isotopes and extremely abnormal Mg-Zn isotopes, and an EMI component constrained by the weakly alkaline basalts with EMI–OIBs' trace-element and isotopic compositions.[26–32] Nonetheless, our results showed that although the Wangjiadashan basalts are weakly alkaline basalts, their melt inclusions have large Pb isotopic variations, which cover the whole Pb isotopic range of the Shandong basalts (Figure 6). More importantly, the melt inclusions from a single lava (sample DSW09-8) exhibit the Pb isotopic values well overlapping the whole Pb isotopic spectrum of the Shandong basalts. Our new Pb isotopic data therefore provide reliable evidence for at least two mantle components in the Wangjiadashan basalts: a LoMu component characterized by low ${}^{20x}Pb/{}^{204}Pb$ but high ${}^{20y}Pb/{}^{206}Pb$ ratios, and an EMII+young HIMU component with higher ${}^{20x}Pb/{}^{204}Pb$ but lower ${}^{20y}Pb/{}^{206}Pb$ ratios. An EMII+young HIMU component for the high ${}^{20x}Pb/{}^{204}Pb$ and low ${}^{20y}Pb/{}^{206}Pb$ in the mantle source of the Wangjiadashan basalts is consistent with the conclusions of young recycled oceanic crust modified by sedimentary carbonate in the mantle source of the strongly alkaline basalts. The coexistence of the two distinct mantle components in the weakly alkaline basalts, as described for the Wangjiadashan melt inclusions, supports a model of differentiation melting within a highly heterogeneous mantle column.[46]

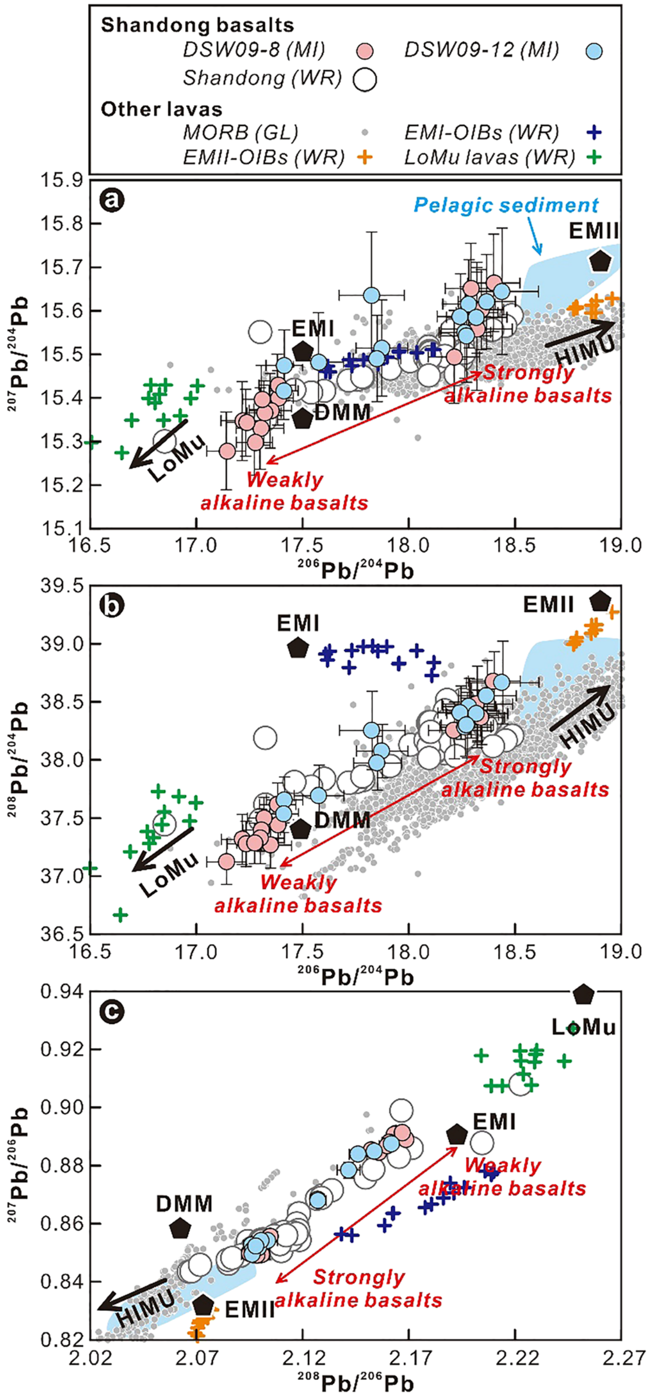

FIGURE 6 Pb isotopic compositions of the Wangjiadashan melt inclusions (MI). References are as follows: Whole-rock (WR) Pb isotopic compositions of the Shandong basalts[20]; whole-rock Pb isotopic compositions of EMI-OIBs (Pitcairn) and EMII-OIBs (Samoan)[20]; pelagic sediment Pb isotopic compositions[43]; glass (GL) Pb isotopic compositions of the global MORB[44]; DMM, EMI, EMII, and HIMU Pb isotopic compositions[9]; LoMu Pb isotopic compositions[18] [Color figure can be viewed at wileyonlinelibrary.com]

4 | CONCLUSIONS

In situ Pb isotope analyses of small low-Pb melt inclusions were undertaken using LA–MC–ICP–MS with ICs simultaneously determining the beam intensities of all Pb isotopes and ${}^{202}Hg$, and an Hg-removal signal-smoothing device to reduce ${}^{204}Hg$ interference with ${}^{204}Pb$. Analyses of the BHVO-2G standard with small laser spot sizes (<100 μm), low energy fluences (3–4 J cm^{-2}), and low repetition rates (3–4 Hz) yielded external precisions and accuracies of Pb isotopic ratios of 2RSD <1% and <0.6% for $^{20x}Pb/^{204}Pb$ and $^{20y}Pb/^{204}Pb$, respectively, with ^{208}Pb intensities of >100 000 cps. Replicate analyses of the ML3B-G, NIST 614, NKT-1G, T1-G, GOR132-G, and StHs6/80-G standards using 32–44 μm spot sizes, 2–4 J cm^{-2} fluence, and 2.5–4 Hz repetition rates yielded external precisions of <0.8% and <0.5% (2RSD) for $^{20x}Pb/^{204}Pb$ and $^{20y}Pb/^{206}Pb$ ratios, respectively. The Pb isotopic ratios of the Wangjiadashan melt inclusions (containing <3 ppm Pb) indicate the coexistence of LoMu and EMII+young HIMU components in the mantle source of the weakly alkaline basalts.

ACKNOWLEDGMENTS

The authors gratefully acknowledge reviews by two anonymous referees, as well as editorial handling by Dr Roland Bol. This work was jointly supported by the NSFC (92055208, 42172053, 42002057), Guangxi Natural Science Foundations of China (GuikeAD22035160), the Key Special Project for Introduced Talents Team of Southern Marine Science and Engineering Guangdong Laboratory (Guangzhou) (GML2019ZD0202), the Guangxi Science Innovation Base Construction Foundation (GuikeZY21195031), Bagui Scholar Innovation Project of Guangxi Province (to 2018XU Jifeng), Guangxi Key Laboratory of Hidden Metallic Ore Deposits Exploration (GKY20-065-17-07, GKY20-065-17-08), and Guilin University of Technology (GUTQDJJ 2020015, GUTQDJJ 2019190). This is a contribution to Guangxi Key Mineral Resources Deep Exploration Talent Highland.

PEER REVIEW

The peer review history for this article is available at https://publons.com/publon/10.1002/rcm.9383.

DATA AVAILABILITY STATEMENT

Data available on request from the authors

ORCID

Yinhui Zhang https://orcid.org/0000-0003-2052-8067
Le Zhang https://orcid.org/0000-0001-9161-0653

REFERENCES

1. Roedder E. Fluid inclusions. *Rev Mineral Geochem Mineral Soc Am*. 1984;12. doi:10.1515/9781501508271
2. Frezzotti ML. Silicate-melt inclusions in magmatic rocks: Applications to petrology. *Lithos*. 2001;55:273-299.
3. Rose-Koga EF, Bouvier AS, Gaetani GA, et al. Silicate melt inclusions in the new millennium: A review of recommended practices for preparation, analysis, and data presentation. *Chem Geol*. 2021;570:120145. doi:10.1016/j.chemgeo.2021.120145
4. McDonough WF, Sun SS. The composition of the earth. *Chem Geol*. 1995;120:223-253.
5. Rudnick RL, Gao S. The composition of the continental crust. In: Holland HD, Turekian KK, eds. *The Crust, Treatise on Geochemistry 3*. Oxford: Elsevier-Pergamon; 2003:1-64.
6. Kogiso T, Tatsumi Y, Nakano S. Trace element transport during dehydration processes in the subducted oceanic crust: 1. Experiments and implications for the origin of ocean island basalts. *Earth Planet Sci Lett*. 1997;148:193-205.
7. Hofmann AW, White WM. Mantle plumes from ancient oceanic crust. *Earth Planet Sci Lett*. 1982;57:421-436.
8. Hofmann AW. Mantle geochemistry: The message from oceanic volcanism. *Nature*. 1997;385:219-229.
9. Hofmann AW. Sampling Mantle Heterogeneity through Oceanic Basalts: Isotopes and Trace Elements. In: Holland HD, Turekian KK, eds. *The mantle and Core, Treatise on Geochemistry 2*. Oxford: Elsevier-Pergamon; 2003:61-101.
10. Stracke A, Hofmann AW, Hart SR. FOZO, HIMU, and the rest of the mantle zoo. *Geochem Geophys Geosyst*. 2005;6(5):Q05007. doi:10.1029/2004GC000824
11. Jackson MG, Hart SR, Konter JG, et al. Helium and lead isotopes reveal the geochemical geometry of the Samoan plume. *Nature*. 2014;514:355-358.
12. Koornneef JM, Nikogosian I, Bergen MJ, Vroon PZ, Davies GR. Ancient recycled lower crust in the mantle source of recent Italian magmatism. *Nat Commun*. 2019;10(1):1-10. doi:10.1038/s41467-019-11072-5
13. Zhang L, Ren ZY, Nichols ARL, et al. Lead isotope analysis of melt inclusions by LA-MC-ICP-MS. *J Anal Atom Spectrom*. 2014;29:1393-1405.
14. Saal AE, Hart SR, Shimizu N. Pb isotopic variability in melt inclusions from the EMI–EMII–HIMU mantle end-members and the role of the oceanic lithosphere. *Earth Planet Sci Lett*. 2005;240:605-620.
15. Yurimoto H, Kogiso T, Abe K, Barsczus HG, Utsunomiya A, Maryuama S. Lead isotopic compositions in olivine-hosted melt inclusions from HIMU basalts and possible link to sulfide components. *Phys Earth Planet in*. 2004;146:231-242.
16. Paul B, Woodhead JD, Hergt J. Improved in situ isotope analysis of low-Pb materials using LA-MC-ICP-MS with parallel ion counter and faraday detection. *J Anal Atom Spectrom*. 2005;20:1350-1357.
17. Paul B, Woodhead JD, Hergt J, Danyushevsky L, Kunihiro T, Nakamura E. Melt inclusion Pb-isotope analysis by LA–MC–ICPMS: Assessment of analytical performance and application to OIB genesis. *Chem Geol*. 2011;289(3):210-223.
18. Chen Y, Zhang Y, Graham D, Su S, Deng J. Geochemistry of Cenozoic basalts and mantle xenoliths in Northeast China. *Lithos*. 2007;96:108-126.
19. Woodhead JD, Hergt JM. Strontium, neodymium and lead isotope analyses of NIST glass certified reference materials: SRM 610, 612, 614. *Geostand Newslett*. 2001;25:261-266.
20. GeoReM. Max-Planck-Institute database for geological and environmental reference materials. http://georem.mpch-mainz.gwdg.de/
21. Jochum KP, Wilson SA, Abouchami W, et al. GSD-1G and MPI-DING reference glasses for in situ and bulk isotopic determination. *Geostand Geoanal Res*. 2011;35:193-226.
22. Potts PJ, Thompson M, Wilson S. G-Probe-1—An international proficiency test for microprobe laboratories—Report on round 1: February 2002 (TB-1 basaltic glass). *Geostand Newsl*. 2002;26:197-235.
23. Elburg M, Vroon P, Wagt B, Tchalikian A. Sr and Pb isotopic composition of five USGS glasses (BHVO-2G, BIR-1G, BCR-2G, TB-1G, NKT-1G). *Chem Geol*. 2005;223:196-207.
24. Matthews KA, Murrell MT, Goldstein SJ, Nunn AJ, Norman DE. Uranium and thorium concentration and isotopic composition in five glass (BHVO-2G, BCR-2G, NKT-1G, T1-G, ATHO-G) and two powder (BHVO-2, BCR-2) reference materials. *Geostand Geoanal Res*. 2011;35:227-234.
25. Huang JL, Zhao DP. High-resolution mantle tomography of China and surrounding regions. *J Geophys Res*. 2006;111(B9):B09305. doi:10.1029/2005JB004066
26. Xu YG, Li HY, Hong LB, Ma L, Ma Q, Sun MD. Generation of Cenozoic intraplate basalts in the big mantle wedge under eastern Asia. *Sci China Earth Sci*. 2018;61:869-886.

27. Zeng G, Chen LH, Xu XS, Jiang SY, Hofmann AW. Carbonated mantle sources for Cenozoic intra-plate alkaline basalts in Shandong, North China. *Chem Geol*. 2010;273:35-45.
28. Sakuyama T, Tian W, Kimura JI, et al. Melting of dehydrated oceanic crust from the stagnant slab and of the hydrated mantle transition zone: Constraints from Cenozoic alkaline basalts in eastern China. *Chem Geol*. 2013;359:32-48.
29. Li HY, Xu YG, Ryan JG, et al. Olivine and melt inclusion chemical constraints on the source of intracontinental basalts from the eastern North China craton: Discrimination of contributions from the subducted Pacific slab. *Geochim Cosmochim Acta*. 2016;178:1-19.
30. Wang ZZ, Liu SA, Chen LH, Li SG, Zeng G. Compositional transition in natural alkaline lavas through silica-undersaturated melt–lithosphere interaction. *Geology*. 2018;46(9):771-774. doi:10.1130/G45145.1
31. Zeng G, Chen LH, Hofmann AW, et al. Nephelinites in eastern China originating from the mantle transition zone. *Chem Geol*. 2021;576: 120276.
32. He YS, Meng XN, Ke S, et al. A nephelinitic component with unusual δ^{56}Fe in Cenozoic basalts from eastern China and its implications for deep oxygen cycle. *Earth Planet Sci Lett*. 2019;512:175-183.
33. Li HY, Taylor RN, Prytulak J, et al. Radiogenic isotopes document the start of subduction in the Western Pacific. *Earth Planet Sci Lett*. 2019; 518:197-210.
34. Zeng G, Chen LH, Hofmann AW, Jiang SY, Xu XS. Crust recycling in the sources of two parallel volcanic chains in Shandong, North China. *Earth Planet Sci Lett*. 2011;302:359-368.
35. Xu Z, Zhao ZF, Zheng YF. Slab-mantle interaction for thinning of cratonic lithospheric mantle in North China: Geochemical evidence from Cenozoic continental basalts in Central Shandong. *Lithos*. 2012; 146:202-217.
36. Zhang YH, Ren ZY, Hong LB, Zhang L, Huang XL, Chen LL. Petrogenesis of Cenozoic Wangjiadashan basalts in Changle area, Shandong Province. *Geochimica*. 2016;45(1):1-23. (in Chinese with English abstract).
37. Ren ZY, Ingle S, Takahashi E, Hirano N, Hirata T. The chemical structure of the Hawaiian mantle plume. *Nature*. 2005;436:837-840.
38. Hu Z, Zhang W, Liu Y, et al. A novel "wave" signal-smoothing and mercury-removing device for laser ablation quadrupole and multiple collector icpms analysis: Application to lead isotope analysis. *Anal Chem*. 2015;87(2):1152-1157.
39. Rosman KJR, Taylor PDP. Isotopic compositions of the elements (technical report): Commission on atomic weights and isotopic abundances. *Pure Appl Chem*. 1998;70:217-235.
40. Chen K, Yuan H, Bao Z, Zong C, Dai M. Precise and accurate in situ determination of lead isotope ratios in NIST, USGS, MPI-DING and CGSG glass reference materials using femtosecond laser ablation MC-ICP-MS. *Geostand Geoanal Res*. 2013;38:5-21.
41. Zhang W, Hu ZC, Yang L, et al. Improved inter-calibration of faraday cup and ion counting for in situ Pb isotope measurements using LA-MC-ICP-MS: Application to the study of the origin of the Fangshan pluton, North China. *Geostand Geoanal Res*. 2015;39:467-487.
42. Souders AK, Sylvester PJ. Improved in situ measurements of lead isotopes in silicate glasses by LA-MC-ICP-MS using multiple ion counters. *J Anal Atom Spectrom*. 2008;23:535-543.
43. Cousens BL, Allan JF, Gorton MP. Subduction-modified pelagic sediments as the enriched component in back-arc basalts from the Japan Sea: Ocean drilling program sites 797 and 794. *Contrib Mineral Petrol*. 1994;117(4):421-434. doi:10.1007/BF00307275
44. The Petrological Database of the Ocean Floor (PetDB). http://www.earthchem.org/petdb
45. Jackson M, Hart S, Koppers A, et al. The return of subducted continental crust in Samoan lavas. *Nature*. 2007;448:684-687.
46. Zhang YH, Ren ZY, Hong LB, et al. Differential partial melting process for temporal variations of Shandong basalts revealed by melt inclusions and their host olivines. *Gondw Res*. 2017;49:205-221.

SUPPORTING INFORMATION

Additional supporting information can be found online in the Supporting Information section at the end of this article.

How to cite this article: Yu H, Zhang Y, Liu X, et al. Improved in situ analysis of lead isotopes in low-Pb melt inclusions using laser ablation–multi-collector–inductively coupled plasma–mass spectrometry. *Rapid Commun Mass Spectrom*. 2022; 36(22):e9383. doi:10.1002/rcm.9383